sustainability

MDPI

Article

Autogenous Self-Healing Capacity of Early-Age Ultra-High-Performance Fiber-Reinforced Concrete

Estefania Cuenca [1,*] and Pedro Serna [2]

[1] Department of Civil and Environmental Engineering, Politecnico di Milano, 20133 Milan, Italy
[2] Institute of Concrete Science and Technology (ICITECH), Universitat Politècnica de València, 46022 Valencia, Spain; pserna@cst.upv.es
* Correspondence: estefania.cuenca@polimi.it

Abstract: This paper analyzes the autogenous self-healing capacity of early-age Ultra-High-Performance Fiber-Reinforced concretes (UHPFRCs) by measuring the crack closure and the possible mechanical recovery on healed specimens. The main parameters considered in this research were the healing exposure conditions (humidity chamber, immersion in tap water, immersion in seawater and heat curing) and the precracking levels (microcracks and macrocracks). For the microcrack level, four-point bending tests were performed on prismatic specimens ($100 \times 100 \times 500$ mm^3) obtaining a multiple cracking pattern characterized by crack widths ranged from 10 to 20 μm. Whereas for the macrocrack level (behavior after crack localization), splitting tests were carried out on notched cubic specimens ($100 \times 100 \times 100$ mm^3) obtaining crack widths of up to 0.4 mm. For both precracking levels, specimens were precracked at two days and were cured for one month in the mentioned exposure conditions. Healing products were analyzed on the specimen surface and also inside the cracks; to this purpose, their microstructure was analyzed by means of SEM and EDS analyses. The results have shown that the highest crack closure values were obtained for the heat-cured specimens and for the specimens immersed in water (tap water and seawater) whereas the less efficient condition was the humidity chamber.

Keywords: autogenous healing; early-age concrete; self-healing concrete

Citation: Cuenca, E.; Serna, P. Autogenous Self-Healing Capacity of Early-Age Ultra-High-Performance Fiber-Reinforced Concrete. *Sustainability* **2021**, *13*, 3061. https://doi.org/10.3390/su13063061

Academic Editor: José Ignacio Alvarez

Received: 19 January 2021
Accepted: 16 February 2021
Published: 11 March 2021

1. Introduction

Sustainability is becoming more relevant every day in the field of construction [1]. Sustainability is directly linked to durability which is becoming of paramount importance in the field of reinforced concrete (RC) structures. RC structures should be maintained along all their service life to minimize maintenance and reparation costs. A recent study has shown that reparation tasks of degraded RC due to corrosion have an average yearly global cost of a 3.4% of the global gross domestic product [2]. As a matter of fact, new cementitious composites are being developing during the last decades to obtain more durable cementitious composites such as the Ultra-High-Performance Fiber-Reinforced Concrete (UHPFRC). These concretes reach compressive strength values higher than 120 MPa and direct tensile strengths between 5 and 10 MPa with very low porosities (lower than 5%) [3–5]. Consequently, UHPFRC present outstanding durability properties in uncracked state due to its low porosity. However, its composition characterized by a low water/cement (w/c) ratio (up to 0.2) confers to concrete a higher risk of early-age cracking due to increased autogenous and drying shrinkage [6–11]. In fact, early-age cracks can have negative effects on durability of RC structures whose consequence could be a shortening of their service life, especially for those structure exposed to chlorides and sulfates rich environments. To avoid or prevent durability problems, early-age cracking can be controlled with rebar reinforcement but also with fibers, shrinkage-reducing additives and nanoadditives, among others [12,13]. The addition of fibers (usually more than 1.5% in volume) confers to concrete a higher ductility [4,6–12]. Although UHPFRC specimens can show strain-softening behavior in some conditions, they generally present hardening behavior (or close to hardening)

in tension due to the favorable alignment of fibers along the longitudinal direction of the specimen. The hardening behavior is distinguished by a multiple microcracking phase after achieving cracking strength and before crack localization [14]. In this context, self-healing techniques could prevent deterioration problems by repairing early-age cracks, trying to regain totally or partially the mechanical [6] and permeability [15] properties after early-age cracking [16]. Self-healing improves concrete durability and hence increases the service life of RC structures by reducing the maintenance and reparation tasks [17], guaranteeing adequate long-term behavior of RC structures. Although research on self-healing of early-age cracks has been carried out [9,18–20], it has been observed that the majority of these studies are focused on microcracks (crack openings lower than 150 μm) whereas the self-healing analysis on early-age macrocracks wider than 300 μm has been less studied [21,22]. The study of macrocracks is particularly interesting based on the findings observed by Wang et al. [23] in which they ensured that the permeability of cementitious materials with microcracks smaller than 50 μm were similar to undamaged materials. Regarding early-age microcracks, Darquennes et al. [18] found that blast-furnace slag has an important ability of ongoing hydration at early age (<28 days) and their anhydrate particles allocated inside cracks allowed hydration after cracking. Yang et al. [9] damaged the specimens in direct tension after three days, obtaining crack widths less than 60 μm. In this context, specimens exposed to environments in presence of water showed good self-healing properties at early ages. Specifically, they found that the most relevant factor to activate self-healing in early-age cracks is the contact with water, permanently immersed or subjected to cycles. Moreover, higher levels of recovery in resonant frequency test and stiffness were observed when cracks were below 50 μm. According to their results, self-healing should maintain stiffness, strength and ductility when preloading strain is limited to 0.3%. Shim et al. [19] cracked their specimens after seven days, reaching cracks up to 300 μm, and they found that the incorporation of superabsorbent polymers (SAP) can improve the autogenous healing of concrete specimens subjected to wet/dry cycles. On the other hand, regarding early-age macrocracks (>300 μm), Roig-Flores and Serna [22] precracked cylindrical concrete specimens two days after casting up to 0.1 and 0.4 mm; then, specimens were subjected to wet/dry cycles, humidity chamber and water immersion. Complete crack sealing for cracks smaller than 0.15 mm and a partial crack closure for cracks width from 0.15 to 0.35 mm were detected. For larger cracks (>0.4 mm), the crack–closing ratio was clearly reduced. Moreover, a complete sealing under wet/dry cycles was reached for cracks up to 0.10 and 0.25 mm after 7 and 42 days of healing, respectively. Analogously, specimens immersed in water reached complete closure for cracks up to 0.16 and 0.32 mm after 7 and 42 days of healing, respectively. It was also observed that autogenous healing sealed the cracks on their surface but not internally. Hong et al. [21] studied the autogenous healing of early-age cracks in cementitious materials with superabsorbent polymers (SAP). To this purpose, specimens were cracked seven days after casting to be then subjected to wet/dry cycles and to wet conditions. Based on the water flow rates obtained, it was observed that 1% of SAP can completely interrupt the water flow through cracks up to 300 μm in early-age cracks.

The aim of this research is to evaluate the autogenous self-sealing and the self-healing capacity of an early-age Ultra-High-Performance Fiber-Reinforced Concrete (UHPFRC). Few studies are present in the literature regarding self-healing in UHPFRC [12,24,25]. To this purpose, specimens were precracked at different levels (microcracks of 10–20 μm and macrocracks of up to 0.4 mm). With the microcrack level, the behavior before the crack localization was analyzed whereas with the macrocrack level the behavior of the localized crack was studied. Then, they were subjected to humidity chamber, heat curing and water immersion (tap and seawater) for one month to promote self-healing of cracks. To evaluate the self-sealing ability, the crack width was measured before and after the healing periods by means of a digital microscope to analyze the crack closure on the surface of the specimen. In addition, self-healing efficiency was analyzed by means of tensile and flexural strength tests to evaluate the possible mechanical recovery on healed specimens. Finally,

the morphology and chemical composition of the healing products formed in the several exposure conditions were analyzed by means of microstructural analyses to also verify their presence outside and inside the crack to guarantee self-sealing and/or self-healing.

2. Materials and Methods

2.1. Aim of the Research

The aim of this research is to evaluate the autogenous self-sealing and the self-healing capacity of an early-age Ultra-High-Performance Fiber-Reinforced Concrete (UHPFRC). For this purpose, a methodology consisting of four phases was adopted. Firstly, specimens were casted and cured; secondly, specimens were precracked to create a controlled damage in the specimens; thirdly, specimens were exposed to different environments to promote healing of cracks; and finally, self-sealing and self-healing ability were quantified in terms of crack closure and mechanical recovery, respectively. It is important to highlight that particular attention has been paid to the cracks generated before and after crack localization. It is well known that the hardening behavior is distinguished by a multiple microcracking phase after achieving cracking strength and before crack localization [14]. In this research, self-sealing and self-healing of cracks have been studied on microcracks (10–20 μm) and macrocracks (0.4 mm), before and after crack localization, respectively.

2.2. Materials and Mix Design Proportions

The experimental program was carried out focusing on an Ultra-High-Performance Fiber-Reinforced Concrete (UHPFRC), whose composition is detailed in Table 1. The cement used was a sulfate-resistant Portland cement (type I), CEM I 42.5 R-SR5 from Lafarge® (Zug, Switzerland), which allowed high strength values with high initial strength values, according to the Standard EN 197-1, and it was ideal for the manufacture of sulfate resistant concrete. The water/cement ratio (w/c) was equal to 0.2. Two siliceous sand types were added, a fine sand with a maximum diameter size of 0.5 mm and a medium sand with maximum diameter sizes ranging from 0.6 to 1.2 mm. To obtain a continuous particle size distribution, siliceous fine powder from Sibelco® (Antwerp, Belgium) (Quarzfin U-S 500) was added. Moreover, microsilica fume from Elkem® (Oslo, Norway) was added to reach higher mechanical strength values and to densify the concrete matrix diminishing the concrete permeability. This fact allows to obtain a more durable concrete, and hence more sustainable one. The superplasticizer Sika® (Baar ZG, Switzerland) 20HE was used to obtain a higher level of workability. Cracking control was beneficial to arrest crack openings and hence to improve healing ability of the cracks. To this end, a large amount (175 kg/m^3) of bright straight high carbon wire micro-steel fibers Dramix® (Zwevegem, Belgium) OL was used to control cracking during the precracking tests. The micro-steel fibers used in this research had the following characteristics: diameter = 0.22 mm; length = 13 mm; aspect ratio (length/diameter) = 59; nominal tensile strength = 2750 MPa and Young's modulus = 200 GPa. With reference to this and to guarantee a good dispersion of such a high amount of steel fibers in the concrete, the following mixing protocol was followed: 1. Dry mixing of fine and medium sand; 2. Dry mixing of cement, microsilica fume and siliceous fine powder; 3. Add water; 4. Add superplasticizer; 5. Add micro-steel fibers.

Table 1. Mix design of Ultra-High-Performance Fiber-Reinforced Concrete (UHPFRC).

Constituent	kg/m^3
Cement CEM I 42.5 R-SR5 Lafarge®	800
Microsilica fume 940 D Elkem® Undensified	175
Siliceous fine powder (Quarzfin from Sibelco®) U-S 500	225
Fine sand (0.5 mm)	302
Medium sand (0.6–1.2 mm)	565
Water	160
Superplasticizer Sika 20HE	30
Micro-steel fibers OL 13/0.22	175

2.3. Experimental Program

The experimental campaign was carried out on unnotched prismatic specimens ($100 \times 100 \times 500$ mm^3) and on notched cubic specimens ($100 \times 100 \times 100$ mm^3). Figure 1 shows the four-point bending test and splitting test setup. In Figure 1b–d it can be observed that the cubes had two deep notches (10 mm deep) originating from the groove vertices, perpendicularly to the ligament (52.5 mm) along which act the tensile stresses. The shape on the front and rear faces was based on DEWS [26] but in this research a cubic geometry ($100 \times 100 \times 100$ mm^3) was chosen. After casting, all the specimens were cured in the molds for 24 h inside the laboratory and then kept in a humidity chamber (20 °C and 100% RH) for one more day. After that, unlike reference samples (without crack), specimens were precracked 2 days after casting up to the two following precracking levels:

- Microcrack (unnotched four-point bending tests on prismatic specimens as in [14] with 450 mm span) for the analysis of diffused cracks of 10–20 μm;
- Macrocrack (splitting tests on notched cubes as in [26] to analyze localized cracks) considering cracks around 0.4 mm.

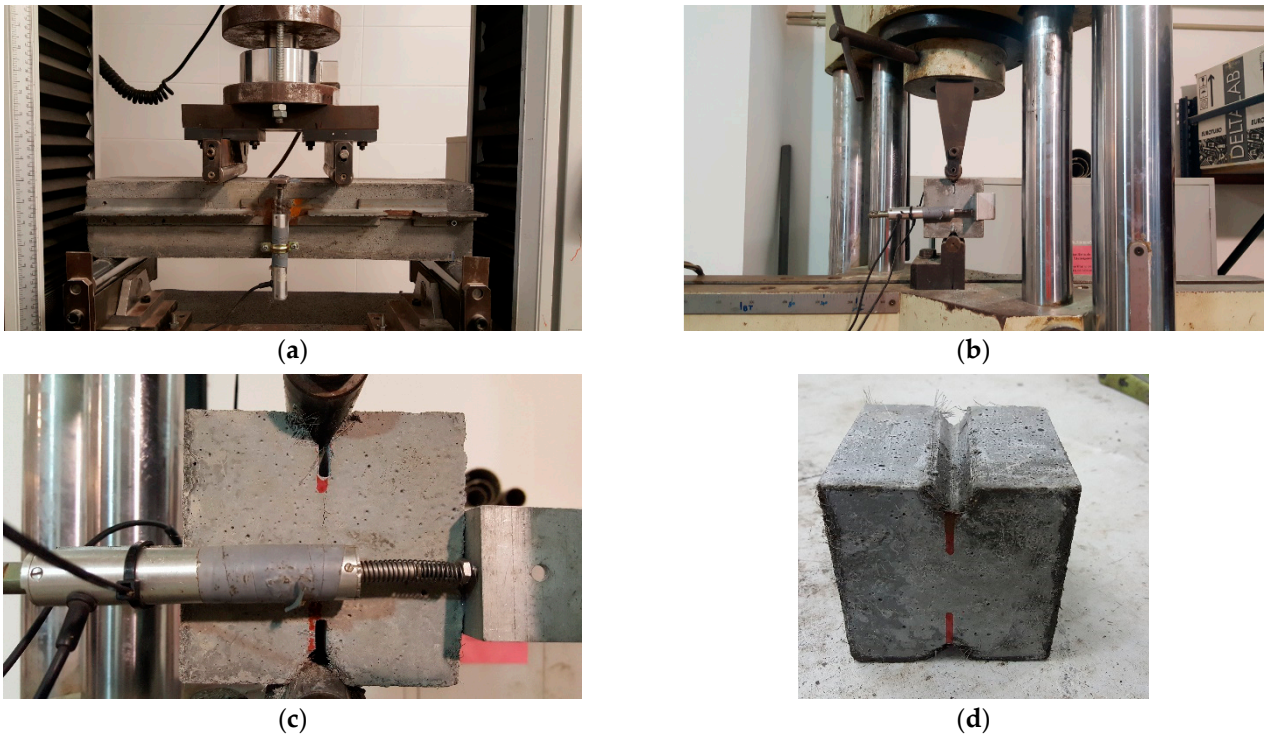

Figure 1. Flexural and splitting test setup: microcrack level in prismatic specimens (**a**) and macrocrack level on notched cubic specimens (**b**–**d**).

After precracking, specimens were subjected to the following exposure conditions for 1 month to promote crack healing:

- Humidity chamber (C): at a constant temperature of 20 °C and 100% relative humidity (RH);
- Immersion in tap water (TW): Immersion in tap water at 25 °C;
- Immersion in seawater (SW): Immersion in an artificial seawater at 25 °C. The artificial seawater was prepared in accordance with the composition indicated in ASTM D1141-98 (2013), as shown in Table 2;
- Heat curing (HC): Specimens were immersed in tap water at 90 °C for 2 days followed by 28 days in a humidity chamber (20 °C, 100% RH).

Table 2. Chemical composition of artificial seawater according to ASTM-D1141-98 (2013).

Chemical Component	Concentration (g/L)
NaCl	24.72
KCl	0.67
$CaCl_2 \cdot 2H_2O$	1.36
$MgCl_2 \cdot 6H_2O$	4.66
$MgSO_4 \cdot 7H_2O$	6.29
$NaHCO_3$	0.18

As reference, three additional specimens were repaired by filling the cracks with an epoxy resin product. This fact allowed to compare self-healing technologies with traditional repairing methods. Table 3 summarizes the experimental program carried out in this research, including the number of specimens tested for each case. After the conditioning, the specimens were visually inspected for crack closure and re-tested with the purpose to evaluate the crack repairing efficacy and the recovery of both stiffness and load-bearing capacity.

Table 3. Experimental program: number of specimens tested in any exposure condition.

Exposure Condition	Prismatic Specimen 100 × 100 × 500 mm³ (4-Point Bending Test: Microcrack Level)		Notched Cube 100 × 100 × 100 mm³ (Splitting Test: Macrocrack Level)	
	Without precrack	Microcrack (10–20 μm)	Without precrack	Macrocrack (up to 0.4 mm)
Humidity chamber (C)	2	3	3	3
Tap water immersion (TW)	-	-	3	3
Seawater immersion (SW)	2	3	3	3
Crack reparation with epoxy resin	-	-	-	3
Heat curing (HC)	2	2	3	3

2.4. Test Methods

2.4.1. Concrete Properties on Fresh and Hardened State

Concrete workability on fresh state was characterized by means of the slump flow test according to the Standard EN 12350-2. Moreover, compressive strength tests were performed on 6 cylindrical specimens (Φ150 mm × 300 mm) casted according to the Standard EN 12390-2. After casting, concrete was cured into the mold for 24 h and after demolding cylinders were cured for 28 days in a humidity chamber (T = 20 °C, RH = 100%) to be tested in compression according to EN 12390-3. In addition, flexural strength tests were performed on prismatic specimens (100 × 100 × 500 mm^3) by means of a four-point bending test carried out with a span of 150 mm and a loading span of 150 mm. In the precracking tests, the test speed was kept constant and equal to 0.05 mm/min before the crack localization, then after the crack localization, it was increased up to 0.15 mm/min.

2.4.2. Precracking Methodology

As briefly explained in Section 2.3, unlike reference samples, specimens were precracked at an early age after casting (2 days). As already underlined, specimens were precracked at two different levels: microcrack and macrocrack level. With the microcrack level it was intended to study the microcracks that are generated before the crack localization, whereas with the macrocrack level the purpose was to analyze the localized crack. The specimens made with UHPFRC showed a hardening behavior characterized by a multiple microcracking phase after reaching cracking strength and before crack localization [27–31]. The crack localization instant happens when one crack widens more than other cracks do [14,32,33].

As explained in Section 2.3, for the microcrack level, 4-point bending tests (Figure 1a) were performed on prismatic specimens (100 × 100 × 500 mm^3) obtaining a multiple cracking pattern along the middle third of the span length with crack widths ranging from 10 to 20 μm, whereas for the macrocrack level, indirect tensile (splitting) tests (Figure 1b–d)

were carried out on notched cubic specimens (100 × 100 × 100 mm^3) obtaining a main crack with an opening up to 0.4 mm. Crack widths were controlled by means of Linear Variable Differential Transformers (LVDTs). In the case of flexural tests, the LVDT measured the deflection in the center of the specimen and in the case of the notched cubes, two LVDT were placed on each side of the specimen measuring the crack width at mid-height of the cube. Figure 2 shows the aspect of the central span of one of the prismatic specimens tested up to failure. Well before the crack localization, microcracks are not visible without the digital microscope. Therefore, the cracks in Figure 2 have been retouched to facilitate the cracking pattern observation to the reader. In this way, in Figure 2 it is possible to observe the multiple instances of microcracking and the localized crack.

Figure 2. Typical final crack pattern observed on the bottom surface after 4-point bending test.

2.4.3. Crack Width Analysis

Self-sealing of the cracks was observed after the different healing exposures by means of a digital microscope Dinolite® (NN Almere, The Netherlands). The digital microscope and its software allowed us to take pictures of the crack at different magnifications (Figure 3). With the microscope, eight pictures were taken for each crack before subjecting specimens to the several environments. These eight pictures allowed us to cover the whole crack. To analyze the same areas before and after the healing exposures, the contour of the microscope was marked into the specimens for each position selected for each picture, as showed in Figure 3a. Calibrating the microscope, it was possible to quantify all the parameters related to the geometry of the crack and the extension of healing products on the surface of the specimens, as shown in Figure 4. As already explained, microcracks were not visible to the naked eye, because of this they were retouched in Figure 4a to facilitate cracking pattern observation to the reader. On the other hand, macrocracks were visible to the naked eye, therefore, they did not need to be retouched in Figures 3 and 4b. It can be observed that, in the notched cubes appeared a localized crack surrounded by other cracks as expected considering the hardening behavior of this kind of concretes (UHPFRC). A full description of the methodology can be found in [15]. In this case, crack width was measured before and after healing period and with these values, it was possible to calculate the crack closure (in %) as indicated in Equation (1):

$$Crack\ closure\ (\%) = \left(\frac{w_{before\ healing} - w_{after\ healing}}{w_{before\ healing}} \right) \times 100 \quad (1)$$

where $w_{before\ healing}$ is the crack width before healing (just after precracking the specimen) and $w_{after\ healing}$ is the crack width after healing the specimens in the different conditions for 1 month.

(**a**)

(**b**)

Figure 3. Crack observation by means of digital microscope: Specimens with circle marks for taking pictures with the digital microscope (**a**) and a picture during the crack evaluation (**b**).

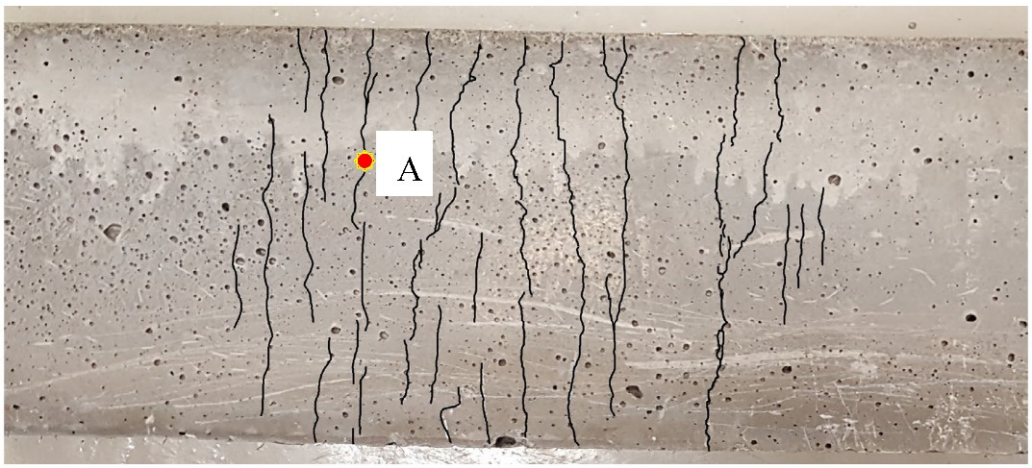

(**a**) Microcrack level at middle third of the span length

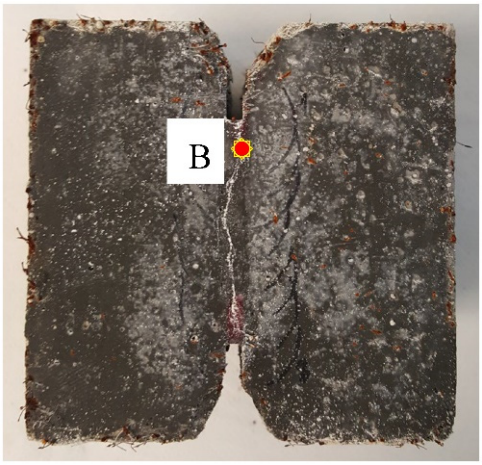

(**b**) Macrocrack level

Figure 4. *Cont.*

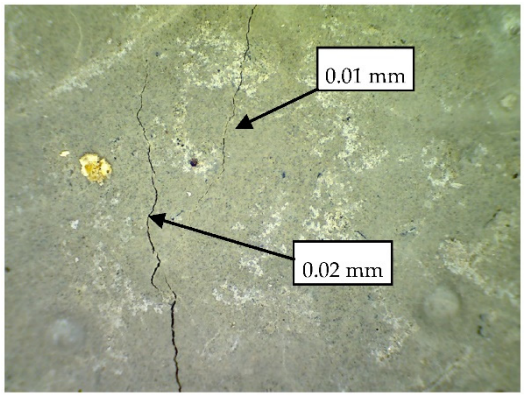

(**c**) Before healing (microcrack at point A)

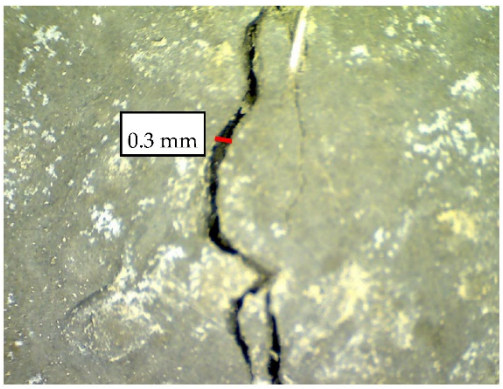

(**d**) Before healing (macrocrack at point B)

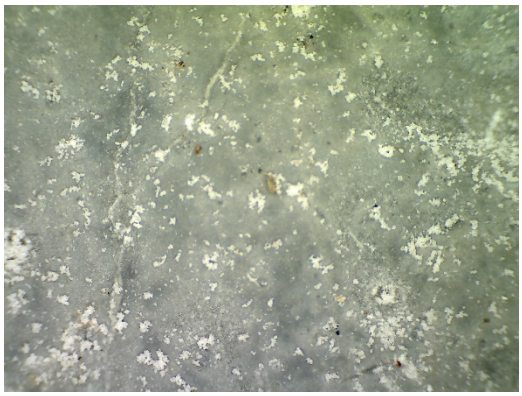

(**e**) After healing (microcrack at point A)

(**f**) After healing (macrocrack at point B)

Figure 4. Crack aspect of micro and macrocracks (before and after healing).

2.4.4. SEM and EDS Analysis

The microstructure of the healing products was studied by means of Scanning Electron Microscope (SEM) analyses, since it is expected that they could be different for each exposure condition. SEM analyses were taken from specimens after being subjected to the different healing exposures used for this research. From each exposure condition, a small sample of 10 × 10 × 10 mm^3 was removed from one of the specimens. Each sample was selected, including part of the macrocrack, in order to analyze the healing products deposited outside and inside the crack. Energy-dispersive X-ray spectroscopy (EDS) analyses were also performed to distinguish the main elements present in the healing products and they were conducted contemporaneously with the SEM analysis.

3. Experimental Results

3.1. Fresh and Hardened-State Properties

The procedures adopted to carry out the mechanical characterization of the UHPFRC used in this research were described in Section 2.4. The slump flow obtained was 650 mm, which corresponds to a SF1 consistency class and the average compressive strength was 139.07 MPa at 28 days, with a coefficient of variation (CoV) of 7.7%. Flexural strength was evaluated by means of four-point bending tests in prismatic specimens (100 × 100 × 500 mm^3). These prisms were tested up to failure 2 days after casting (two prisms) and 28 days after casting (three prisms). The early age of 2 days corresponds to the age selected for precracking the specimens and 28 days was selected to characterize mechanically the UHPFRC used in this work. Figure 5 shows the stress-deflection curves and Table 4 shows the stress at first cracking and the stress at the peak value for both ages, 2 and 28 days. In Figure 5, the star indicates the crack localization initiation which is above

95% of the maximum strength. This is consistent with the findings of López et al. [14] who ensured, after analyzing a comprehensive database, that the analytical crack localization point ranged from 75 to 100% of the flexural strength. In 70% of the cases observed, the crack localization point was greater than 95% of the maximum strength, being the most frequent value at 97% of the maximum strength. In Table 4, it can be observed that at early age (2 days) the specimens showed higher coefficient of variation values than at 28 days.

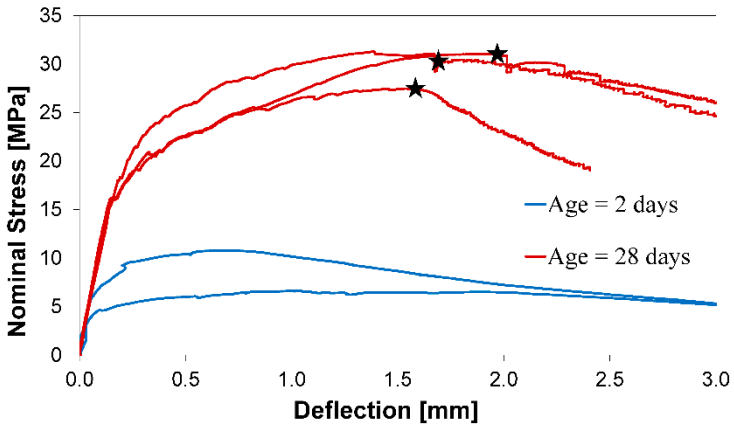

Figure 5. Stress (MPa) versus deflection (mm) curves obtained from flexural tests (the star indicates the initiation of the crack localization).

Table 4. Stress at first cracking (σ_{cr}) and peak stress values (σ_{peak}).

	Stress at First Cracking (σ_{cr})		**Peak Stress (σ_{peak})**	
Concrete Age (days)	2	28	2	28
Average (MPa)	5.23	15.83	8.72	29.93
Coefficient of variation, CoV (%)	16.78	2.66	33.80	7.12

3.2. Crack Sealing Analysis

Once the results obtained from the indirect tensile tests were analyzed, it was observed that the temperature and the continuous immersion in water were essential variables to promote autogenous healing, and their combination increased remarkably the crack sealing ability quantified by means of the crack closure (%), as shown in Figure 6.

It is well known that crack closure (%) is inversely proportional to the initial crack width (the red line in Figure 6 indicates the average trend) [16]. Moreover, it is important to highlight that, although it is well known that in direct tension Ultra-High-Performance Fiber-Reinforced Concretes (UHPFRC) show strain-hardening and multicracking behavior, a main crack was generated along the ligament (with a nominal crack width of up to 0.4 mm). As expected, these macrocracks closed slightly after the downloading branch, reaching maximum residual crack width values up to 0.34 mm, as shown in Figure 6. The highest rates of crack closure were reached in full immersion conditions (tap water and seawater at 25 °C) and also for the heat curing condition (immersion in tap water at 90 °C for 2 days and then placed in the humidity chamber for 28 days). The maximum crack width totally sealed (crack closure = 100%) was equal to 0.2386 mm (for tap water immersion), 0.2109 mm (for heat-cured specimens), 0.2025 mm (for seawater immersion) and 0.027 mm (for humidity chamber). The humidity chamber resulted in the most unfavorable exposure condition to promote self-sealing as the maximum sealable crack width was only equal to 27 μm (0.027 mm). Moreover, the results have demonstrated that the increase of temperature is an accelerating parameter to promote self-sealing. In fact, analogous sealing rates were observed for specimens immersed for only two days in hot water at 90 °C than those immersed for 28 days at 25 °C. As humidity chamber was the worst condition for promoting self-sealing, it could be reasonably thought that for the heat curing exposure,

practically all the achieved sealing develops in the first two days in which specimens were immersed in hot water. Moreover, considering all the ranges of crack widths observed, the highest sealing rates (high crack closure values) were obtained for the heat curing condition followed in decreasing way by tap water immersion, seawater immersion and humidity chamber. As a matter of fact, for a crack width of 0.2 mm (200 µm) the following crack closure (%) average values were obtained: 88% for the heat curing condition, 65 % for the tap water immersion, 45% for the seawater immersion and 20% for the curing in humidity chamber. Moreover, the lowest crack closure (%) value obtained for the heat curing condition was 32% whereas for the other three exposure conditions studied crack closure values equal to zero were also obtained.

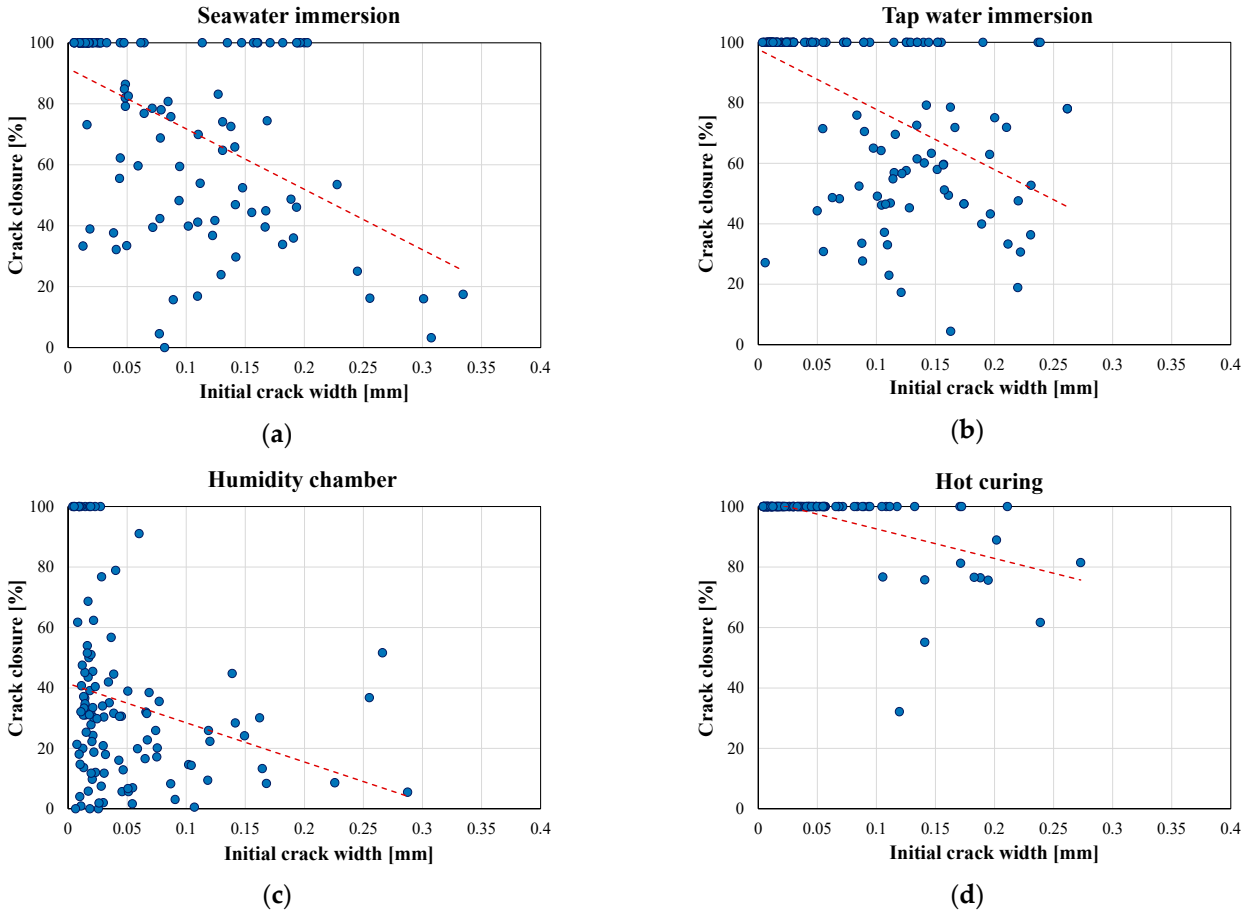

Figure 6. Crack closure (%) versus initial crack width (mm) for the different exposures studies: sea water immersion (**a**), tap water immersion (**b**), humidity chamber (**c**) and heat curing (**d**).

Figures 7 and 8 show the aspect of the eight pictures taken for each macrocrack before and after the different exposure conditions under investigation. All the pictures were taken using the same scale (which is indicated with a red line in Figures 7 and 8). It is important to highlight that the cubic specimens (subjected to indirect tension) developed a multiple cracking behavior although a main macrocrack appeared along the ligament. This range of crack width values allowed to analyze self-sealing of cracks ranging from 0.01 mm to 0.34 mm (Figure 6). For example, this multicracking state can be clearly observed in the pictures of humidity chamber (Figure 7). Moreover, in Figure 6, numerous observation points were analyzed (111 observation points) because there were three cubic specimens for each case, for each specimen eight pictures were taken and for each picture, 4–5 observation points were monitored. This means that, for each cubic specimen, about 37 observation points were analyzed.

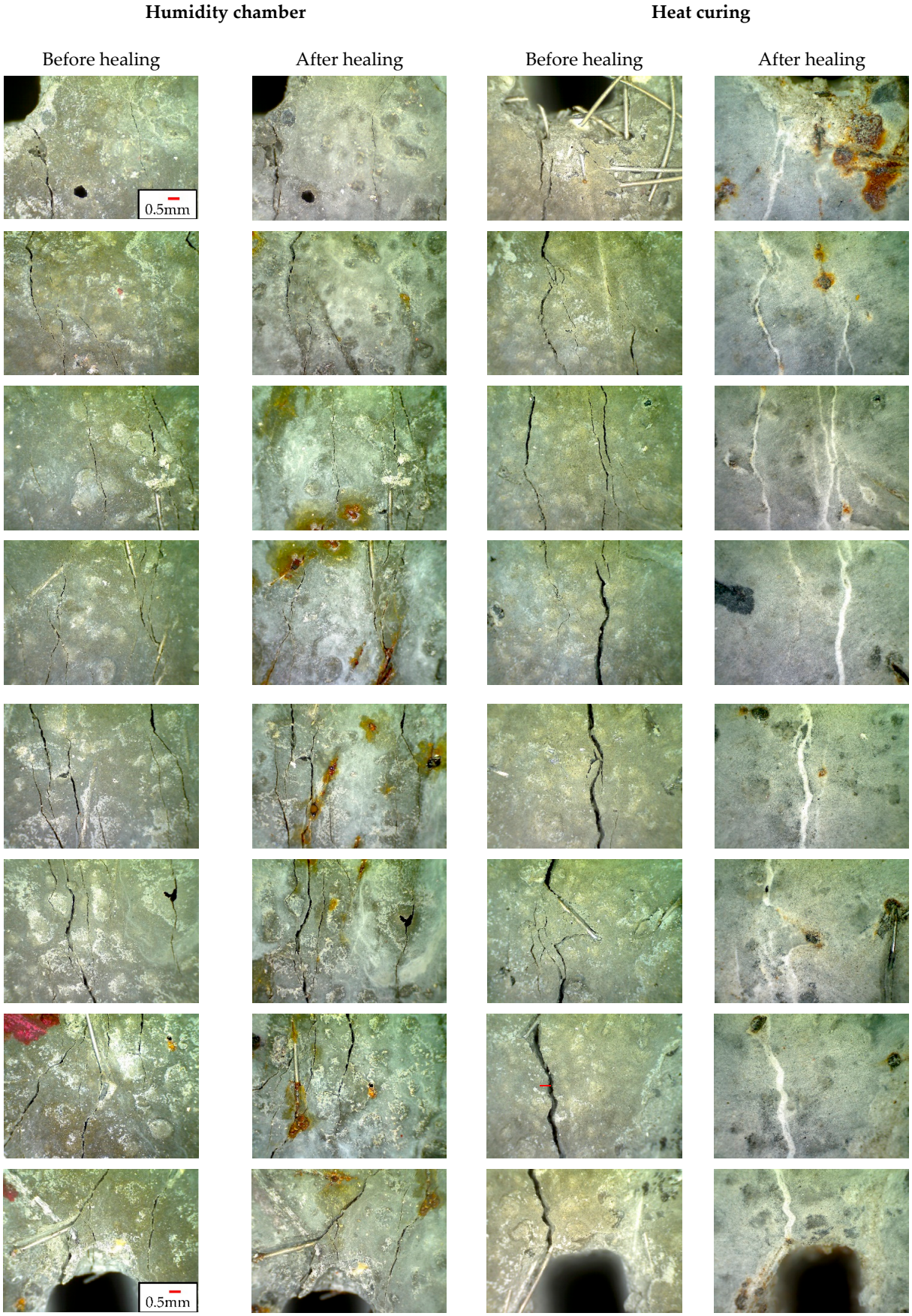

Figure 7. Images of samples before and after healing: humidity chamber and heat curing exposure.

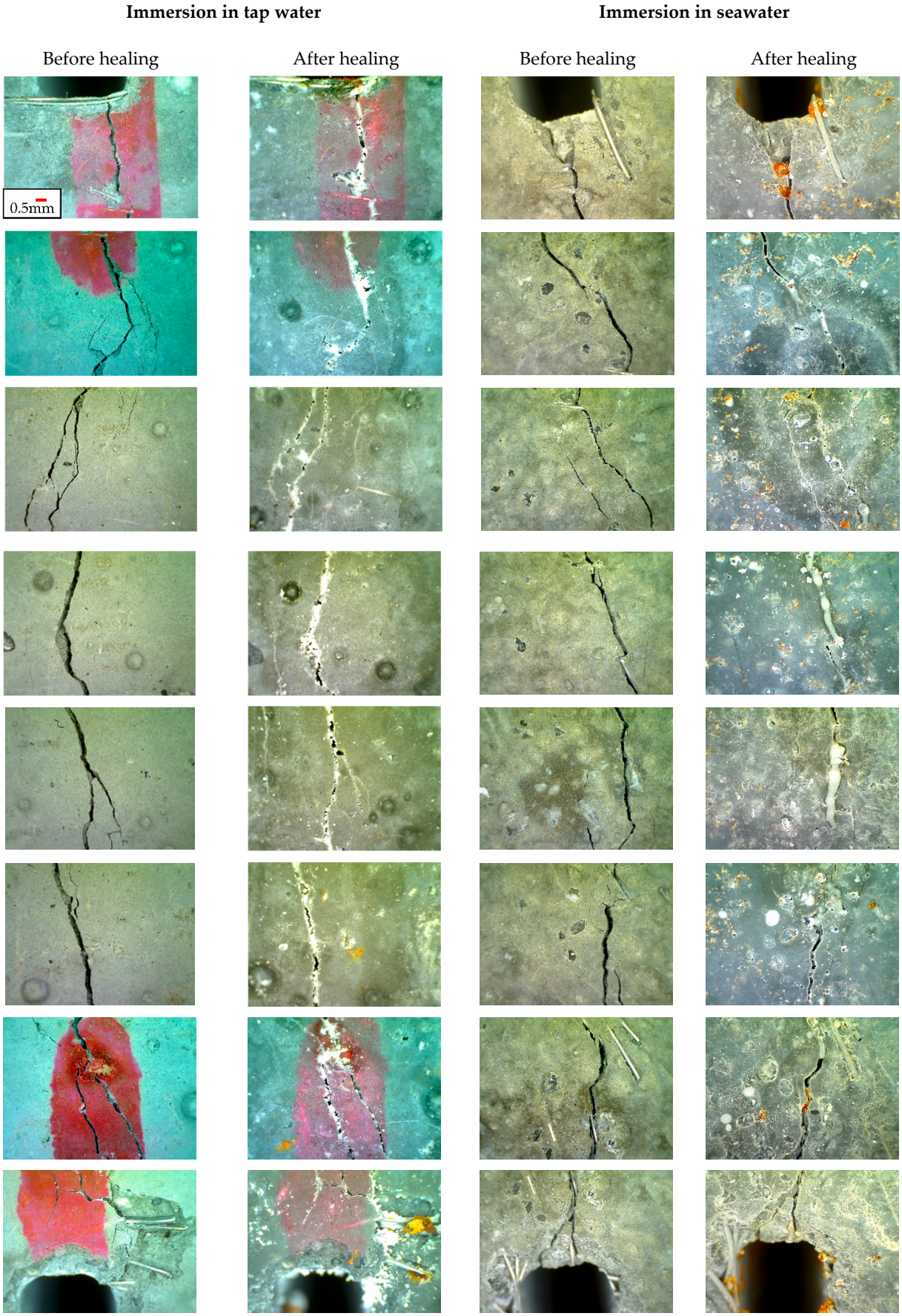

Figure 8. Images of samples before and after healing: immersion in tap water and in seawater.

3.3. Crack Healing (Mechanical Recovery)

As explained previously, two types of tests were carried out to analyze the mechanical response of healed specimens compared to an uncracked specimen of the same age (1 month). From one side, flexural strength tests were conducted, microcracks were numerous and spread in a smeared cracking distribution between the supports being very difficult to detect them visually without a microscope. These cracks were compatible with a serviceability design for traditional concrete. As in this case a single crack did not appear, it was not possible to measure the crack width of each single microcrack. As a matter of fact, a LVDT placed on the midspan of the prismatic specimens (Figure 1a) allowed to measure the deflection during the flexural strength tests by means of four-point bending tests as showed in Figure 9. In Figure 9, the stress versus deflection curves obtained from the four-point bending tests are plotted for each specimen and for each healing exposure. Each single graph contains three curves: one regarding the uncracked specimen with an age of 28 days, one regarding the precracked specimen 2 days after casting and a third one, which is the precracked specimen after the healing period (with an age of 2 + 28 days). The objective is to compare the uncracked one with a healed one of the same age. It is important to highlight that the curves representing the uncracked specimen at 28 days for each exposure conditions come from the same batch and therefore both were analogous specimens. This is the case of C1_28d and C2_28d, SW1_28d and SW2_28d, HC1_28d and HC2_28d. Moreover, the curves C1_28d and C2_28d were analogous to those presented in Figure 5 for the specimens of 28 days.

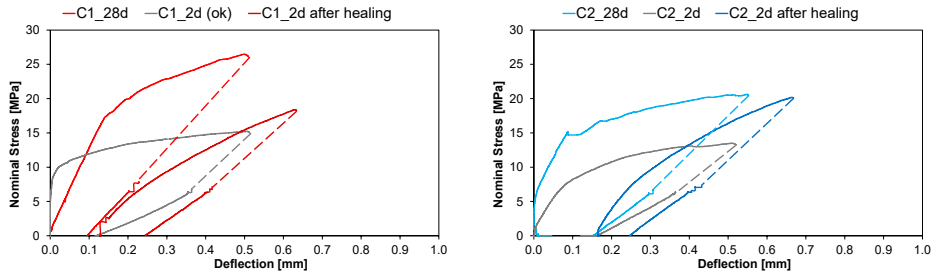

(**a**) Humidity chamber.

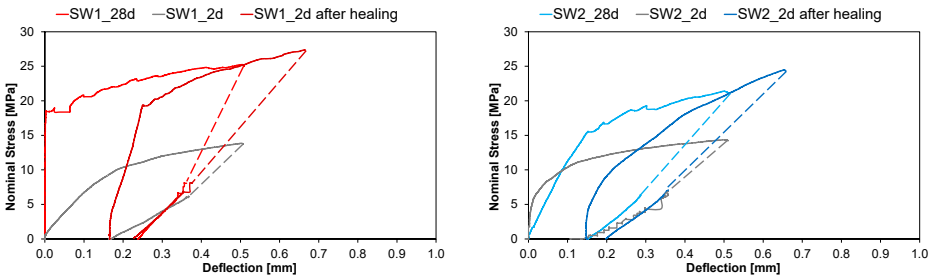

(**b**) Immersion in seawater.

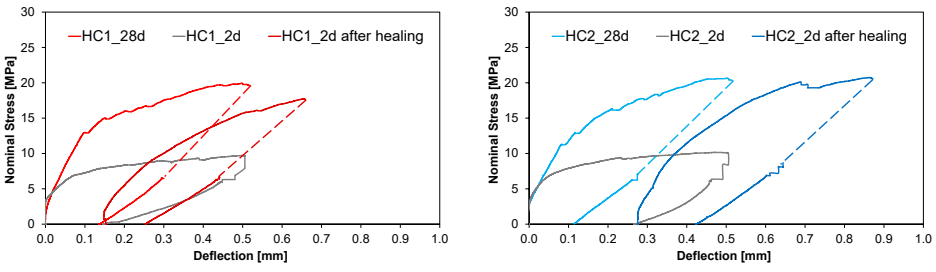

(**c**) Heat curing.

Figure 9. Precracking by means of flexural strength tests up to a microcrack level on prismatic specimens 100 × 100 × 500 mm^3 for specimens cured in humidity chamber (**a**), immersed in sea water (**b**) and heat-cured (c).

From Figure 9, it can be observed that generally all the healed specimens reached the uncracked curve, which means that in this case, microcracks with smaller crack widths (between 10 and 20 μm) can be completely not only sealed but also healed because the fact of been damaged and healed specimens did not suggest a detrimental mechanical performance, as can be observed in Figure 9. In other words, for the studied concretes, a previous microcracking did not condition the residual behavior at 28 days. For all the exposure conditions, the specimens reloaded after healing (2 + 28 days) showed a slower slope (stiffness was not recovered) compared to the uncracked ones but with a similar maximum load capacity. This is not due to self-healing but due to the effect of natural development of maturity that improves the fiber–matrix bond.

On the other hand, indirect tensile strength tests were carried out by means of splitting tests on notched cubes [26]. With these tests, the main objective was to observe which is the self-healing capacity of early-age concretes cracked up to 0.4 mm (400 μm) after being healed for 1 month. Figure 10 shows the mentioned precracking tests showing the curves before and after being healed in the four different exposure conditions. As reference, the results regarding to specimens traditionally repaired with an epoxy resin were included. Figure 10 shows the average Stress versus Crack Opening Displacement (COD) curves obtained from the front and rear face of each notched cube.

From Figure 6 it was observed that macrocracks (close to 0.4 mm) cannot be completely sealed; moreover, from Figure 10 it can be concluded that a macrocrack of 0.4 mm cannot be healed. In fact, in Figure 10 it has been observed that stress–COD curves pertaining to healed specimens were generally below the curves of uncracked samples. This fact means that a width of 0.4 mm (400 μm) is too wide to be completely sealed and healed in such a short healing period, even considering that in our case two positive aspects to promote healing were included as parameters of this research; from one side a concrete with a reduced water/cement ratio (w/c = 0.2) was chosen and, on the other hand, specimens were precracked at an early age (two days). Both aspects promote self-healing because increased the number of cement particles remain anhydrous after mixing. From Figure 10, only mechanical recovery seemed clear in some specimens repaired with epoxy resin. The remaining specimens (regardless of the exposure condition) showed a reduced residual capacity if compared with the equivalent reference specimens at 28 days.

3.4. Microstructural Analysis of the Healing Products

To evaluate the existence of healing products not only in the specimen surface but also inside the crack, microstructural analyses were performed.

Figure 11 shows some micrographs to observe an enlarged image of the cracked area selected for the SEM analysis. In these micrographs medium sand particles, fibers, pores, cracks and some blocks of concrete detached during the precracking test can be clearly distinguished. The surface of the heat-cured specimen showed a different appearance from the specimen cured in a humidity chamber and immersed in seawater.

As explained in the Introduction (Section 1), the main mechanisms to promote autogenous healing are the continuous hydration of anhydrous cement particles and the carbonation of calcium hydroxide. The latter produces calcium carbonate, $CaCO_3$, which can seal or heal the cracks and it is produced when calcium ions from portlandite, $Ca(OH)_2$, react with carbon dioxide, CO_2, present in water, H_2O.

Figure 12 shows the SEM and EDS analyses of the sample belonging to a specimen cured in a humidity chamber where the needles of ettringite (Spectrum 1) and the formation of $CaCO_3$ (Spectrum 2) can be clearly observed. Moreover, the EDS analyses revealed a high peak of Si due to the presence of siliceous sand (SiO_2) in the mix design. On the other hand, healing products on specimens subjected to the most favorable conditions for sealing (immersion in water and heat curing) were also observed (Figures 13 and 14). From Figure 6 it was detected that heat curing and water immersion were the most favorable conditions for sealing cracks, however, in Figure 10, the healing process was not as successful as the sealing process. In order to understand in depth what was happening,

it would be necessary to investigate the distribution of healing products on the crack. To this purpose, SEM and EDS analyses were carried out inside and outside the crack. In Figure 13 are shown SEM observations of a sample from a specimen immersed in seawater, one observation was taken inside the crack and the other outside the crack. It can be observed that outside the crack, the surface had many little cubes, apparently loose, that were very rich of $CaCO_3$, as revealed in its corresponding EDS analysis. This fact would explain the good sealing that was developed on the crack surface. On the other hand, inside the crack those cubes of $CaCO_3$ were not present. These observations would reveal that healing products were deposited mostly on the surface of the crack, promoting crack sealing instead of crack healing.

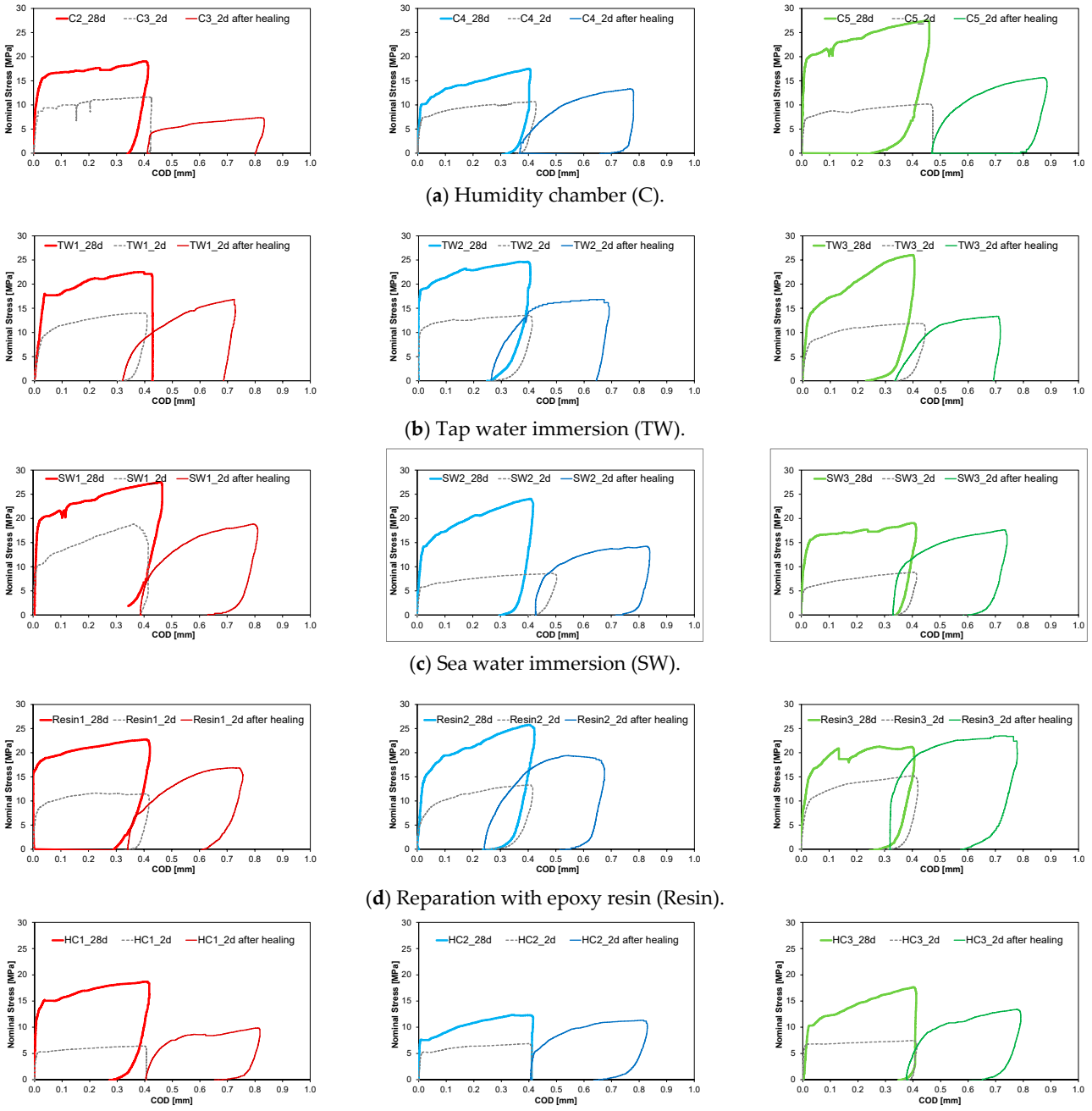

(**a**) Humidity chamber (C).

(**b**) Tap water immersion (TW).

(**c**) Sea water immersion (SW).

(**d**) Reparation with epoxy resin (Resin).

(**e**) Heat curing (HC).

Figure 10. Precracking by means of splitting tests up to a macrocrack level (0.4 mm) on cubic specimens $100 \times 100 \times 100$ mm^3 for specimens cured in humidity chamber (**a**), immersed in tap water (**b**), immersed in seawater (**c**), crack reparation with epoxy resin (**d**) and heat-cured (**e**).

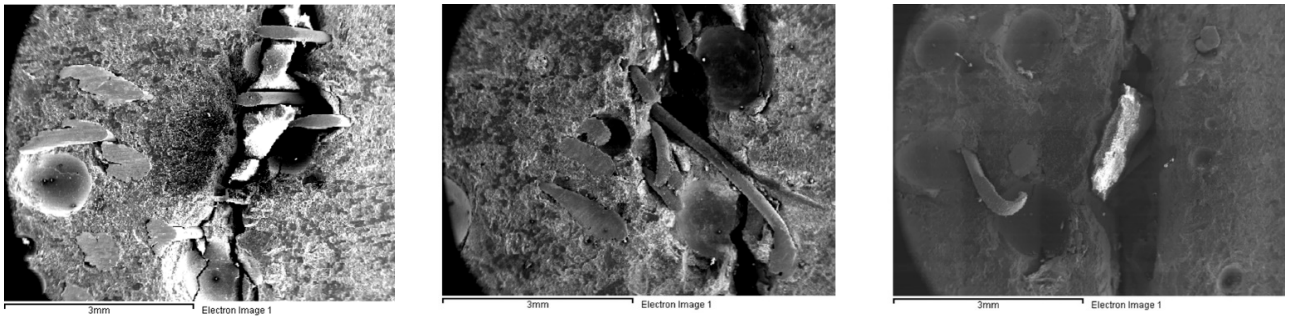

Humidity chamber Seawater Heat curing

Figure 11. Micrographs showing the crack aspect in different curing conditions.

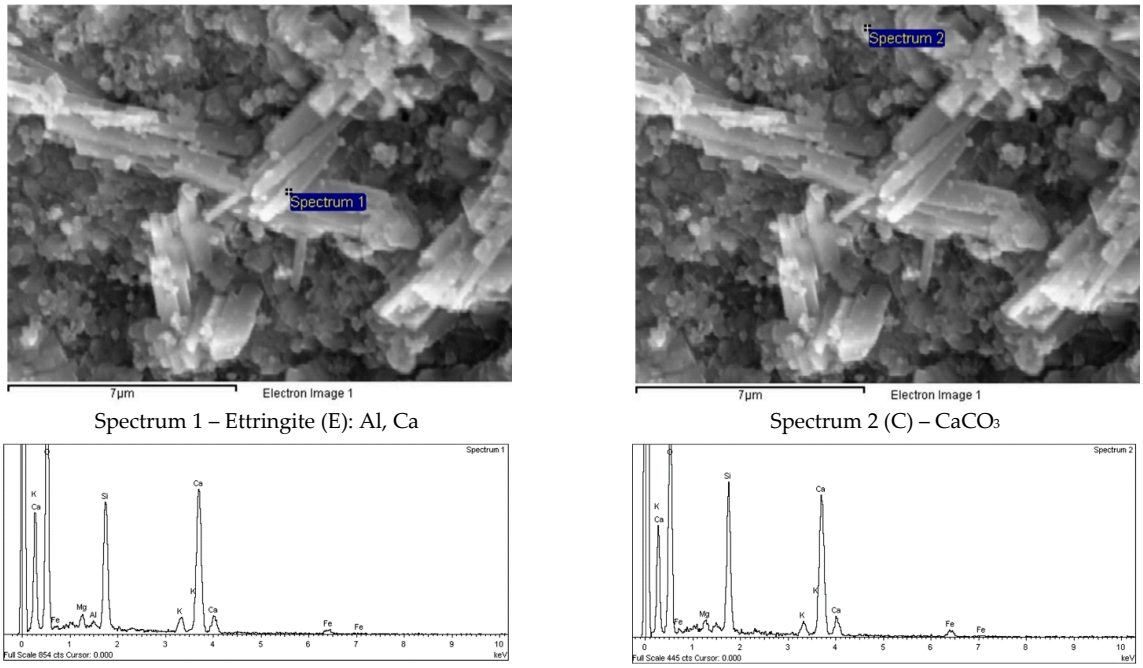

Spectrum 1 – Ettringite (E): Al, Ca Spectrum 2 (C) – $CaCO_3$

Spectrum 1 Spectrum 2

Figure 12. SEM and EDS analysis of a specimen cured in humidity chamber.

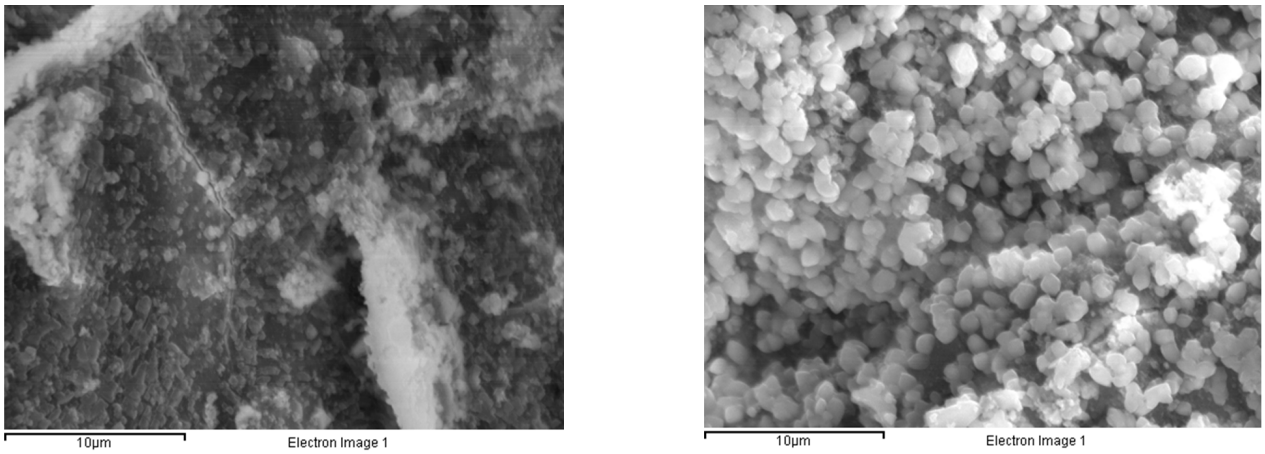

Seawater immersion (inside the crack) Seawater immersion (outside the crack)

Figure 13. *Cont.*

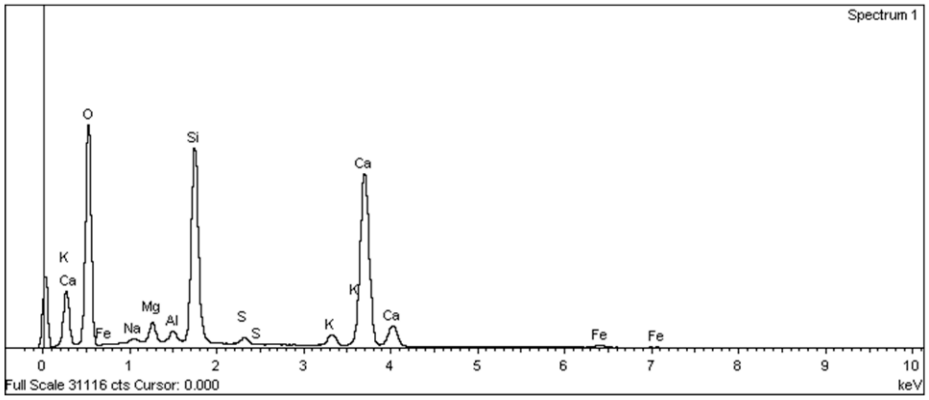

EDS from outside the crack

Figure 13. SEM and EDS analysis of a specimen immersed in seawater.

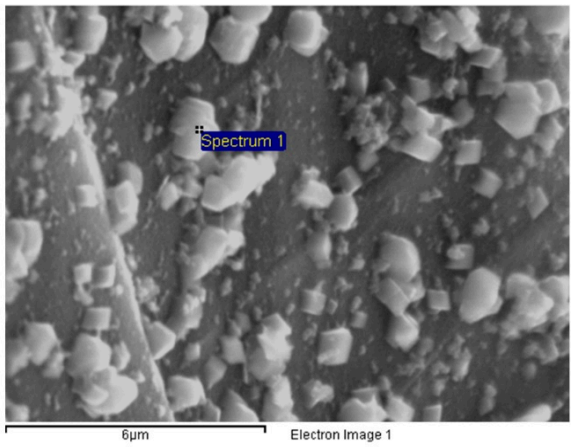

Heat-cured specimen (Left edge of the crack)

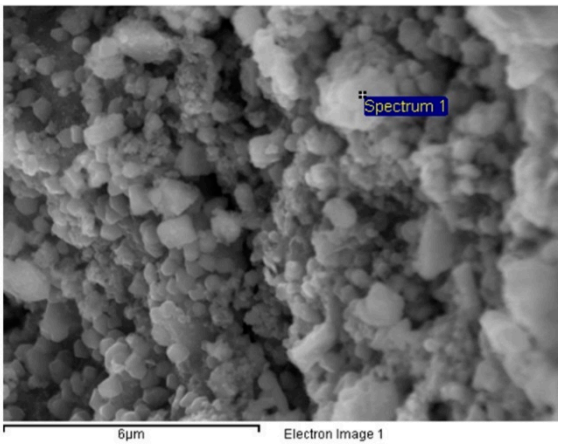

Heat-cured specimen (Right edge of the crack)

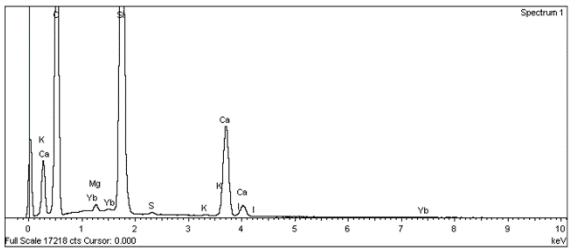

Spectrum 1 (left edge of the crack)

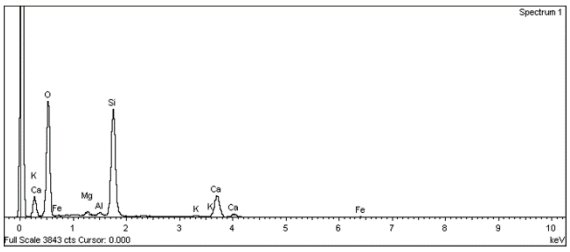

Spectrum 1 (right edge of the crack)

Figure 14. SEM and EDS analysis of a heat-cured specimen.

Figure 14 shows the SEM and EDS analyses carried out on the two edges of the crack for the heat-cured sample. The results from these analyses confirm that healing products were not uniformly distributed along the crack. The right edge was plenty of $CaCO_3$ cubes, whereas in the left edge only some isolated $CaCO_3$ cubes were detected.

4. Conclusions

The aim of this research was to study the autogenous self-sealing and the self-healing capacity of early age of Ultra-High-Performance Fiber-Reinforced Concrete (UHPFRC). To this purpose, specimens were precracked at the early age of two days after casting and were exposed to different exposure conditions for one month. The variables involved in the experimental program were the exposure condition (immersion in tap water or seawater, heat curing treatment and humidity chamber) and the precracking level (microcracks

between 10 and 20 μm and macrocracks of up to 0.4 mm). The main conclusions of this study can be summarized as follows:

- The temperature and the continuous immersion in water were essential variables to promote autogenous healing and their combination increased the crack sealing ability. The highest self-sealing rates were observed for the heat curing condition followed in decreasing order by tap water immersion, seawater immersion and humidity chamber exposure. As a matter of fact, for a crack width of 0.2 mm (200 μm) the following average values of crack closure were reached: 88% for the heat curing condition, 65% for the tap water immersion, 45% for the seawater immersion and 20% for the specimens cured in humidity chamber.
- The widest crack totally sealed was 0.2386 mm for tap water immersion, 0.2109 mm for heat-cured specimens, 0.2025 mm for seawater immersion and 0.027 mm for humidity chamber. The latter was the most unfavorable exposure condition to promote self-sealing/healing.
- Healed specimens (previously precracked by means of flexural tests up to 10–20 μm) reached similar mechanical responses than identical uncracked specimens. The high residual resistance after healing in microcracked specimens was mainly attributed to the maturation of the fiber/matrix bond and not to the self-healing. However, healed specimens (previously precracked by splitting tests up to 0.4 mm) did not reach the mechanical response obtained by identical undamaged specimens because they were only partially healed. This fact was explained through SEM and EDS analyses which showed that healing products were mostly present on the surface of the specimens, whereas they were barely detected inside the cracks.
- In the present research, autogenous healing was not efficient enough to heal completely the macrocracks. On the other hand, microcracks in UHPFRC were clearly sealed and the residual mechanical capacity of the healed specimens was comparable to the uncracked ones.

Author Contributions: Conceptualization, P.S. and E.C.; methodology, P.S. and E.C.; formal analysis, E.C.; investigation, E.C.; data curation, E.C.; writing—original draft preparation, E.C.; writing—review and editing, E.C.; supervision, P.S. All authors have read and agreed to the published version of the manuscript.

Funding: This research activity has been performed in the framework of the 5th call for Short-Term Scientific Missions (STSMs) in the SARCOS (CA 15202) European Cooperation in Science and Technology (COST) Action which covered travel and accommodation costs to the grantee, Estefania Cuenca Asensio. COST is supported by the EU Framework Programme Horizon 2020.

Institutional Review Board Statement: Not applicable.

Informed Consent Statement: Not applicable.

Data Availability Statement: The data that support the findings of this study are available from the corresponding author upon reasonable request.

Conflicts of Interest: The authors declare no conflict of interest.

References

1. Dossche, C.; Boel, V.; De Corte, W.; Van den Heede, P.; De Belie, N. A plant based LCA of high-strength prestressed concrete elements and the assessment of a practical ecological variant. *Cem. Concr. Compos.* **2016**, *73*, 192–202. [CrossRef]
2. Koch, G.; Varney, J.; Thompson, N.; Moghissi, O.; Gould, M.; Payer, J. *International Measures of Prevention, Application and Economics of Corrosion Technologies Study*; NACE International: Houston, TX, USA, 2016.
3. Van Tuan, N.; Ye, G. Hydration and microstructure of ultra high performance concrete incorporating rice husk ash. *Cem. Concr. Res.* **2011**, *41*, 1104–1111. [CrossRef]
4. Wang, W.; Liu, J.; Agostini, F.; Davy, C.; Skoczylas, F.; Corvez, D. Durability of an Ultra High Performance Fiber Reinforced Concrete (UHPFRC) under progressive aging. *Cem. Concr. Res.* **2014**, *55*, 1–13. [CrossRef]
5. Shi, C.; Wu, Z.; Xiao, J.; Wang, D.; Huang, Z.; Fang, Z. A review on ultra high performance concrete: Part I. Raw materials and mixture design. *Constr. Build. Mater.* **2015**, *101*, 741–751. [CrossRef]

6. Cuenca, E.; Ferrara, L. Fracture toughness parameters to assess crack healing capacity of fiber reinforced concrete under repeated cracking-healing cycles. *Theor. Appl. Fract. Mec.* **2020**, *106*, 102468. [CrossRef]
7. Cuenca, E.; Mezzena, A.; Ferrara, L. Synergy between crystalline admixtures and nano-constituents in enhancing autogenous healing capacity of cementitious composites under cracking and healing cycles in aggressive waters. *Constr. Build. Mater.* **2021**, *266*, 121447. [CrossRef]
8. Liu, J.; Farzadnia, N.; Shi, C.; Ma, X. Effects of superabsorbent polymer on shrinkage properties of ultra-high strength concrete under drying condition. *Constr. Build. Mater.* **2019**, *215*, 799–811. [CrossRef]
9. Yang, L.; Shi, C.; Wu, Z. Mitigation techniques for autogenous shrinkage of ultra-high-performance concrete—A review. *Compos. Part B-Eng.* **2019**, *178*, 107456. [CrossRef]
10. Yang, Y.; Yang, E.-H.; Li, V.C. Autogenous healing of engineering cementitious composites at early age. *Cem. Concr. Res.* **2011**, *41*, 176–183. [CrossRef]
11. Wiegrink, K.; Marikunte, S.; Shah, S.P. Shrinkage cracking of high-strength concrete. *ACI Mater. J.* **1996**, *93*, 409–415.
12. Shah, S.P.; Wang, K.; Weiss, W.J. Is high strength concrete durable? In *Concrete Technology for a Sustainable Development in the 21st Century*; CRC Press: Boca Raton, FL, USA, 2000; pp. 102–114.
13. Mihashi, H.; De Leite, J.P.B. State-of-the-art report on control of cracking in early age concrete. *J. Adv. Concr. Technol.* **2004**, *2*, 141–154. [CrossRef]
14. López, J.A.; Serna, P.; Navarro-Gregori, J.; Coll, H. A simplified five-point inverse analysis method to determine the tensile properties of UHPFRC from unnotched four-point bending tests. *Compos. Part B-Eng.* **2016**, *91*, 189–204. [CrossRef]
15. Cuenca, E.; Rigamonti, S.; Gastaldo, E.; Ferrara, L. Crystalline Admixture as Healing Promoter in Concrete Exposed to Chloride-Rich Environments: Experimental Study. *J. Mater. Civ. Eng.* **2021**, *33*, 04020491. [CrossRef]
16. Rooij, M.; van Tittelboom, K.; Belie, N.; Schlangen, E. *Self-Healing Phenomena in Cement-Based Materials: State-of-the-Art Report of RILEM Technical Committee*; Springer: Dordrecht, The Netherlands, 2013; ISBN 9400766246.
17. Maes, M.; De Belie, N. Service life estimation of cracked and healed concrete in marine environment. In Proceedings of the International Conference on Concrete Repair, Thessaloniki, Greece, 20–23 June 2016.
18. Darquennes, A.; Olivier, K.; Benboudjema, F.; Gagné, R. Self-healing at early-age, a way to improve the chloride resistance of blast-furnace slag cementitious materials. *Constr. Build. Mater.* **2016**, *113*, 1017–1028. [CrossRef]
19. Shim, Y.; Hong, G.; Choi, S. Autogenous Healing of Early-Age Cementitious Materials Incorporating Superabsorbent Polymers Exposed to Wet/Dry Cycles. *Materials* **2018**, *11*, 2476. [CrossRef] [PubMed]
20. Roig-Flores, M.; Pirritano, F.; Serna, P.; Ferrara, L. Effect of crystalline admixtures on the self-healing capability of early-age concrete studied by means of permeability and crack closing tests. *Constr. Build. Mater.* **2016**, *114*, 447–457. [CrossRef]
21. Hong, G.; Song, C.; Choi, S. Autogenous Healing of Early-Age Cracks in Cementitious Materials by Superabsorbent Polymers. *Materials* **2020**, *13*, 690. [CrossRef]
22. Roig-Flores, M.; Serna, P. Concrete Early-Age Crack Closing by Autogenous Healing. *Sustainability* **2020**, *12*, 4476. [CrossRef]
23. Wang, K.; Jansen, D.C.; Shah, S.P.; Karr, A.F. Permeability study of cracked concrete. *Cem. Concr. Res.* **1997**, *27*, 381–393. [CrossRef]
24. Yoo, D.Y.; Shin, W.; Chun, B.; Banthia, N. Assessment of steel fiber corrosion in self-healed ultra-high-performance fiber-reinforced concrete and its effect on tensile performance. *Cem. Concr. Res.* **2020**, *133*, 106091. [CrossRef]
25. Kim, S.; Yoo, D.Y.; Kim, M.J.; Banthia, N. Self-healing capability of ultra-high-performance fiber-reinforced concrete after exposure to cryogenic temperature. *Cem. Concr. Compos.* **2019**, *104*, 103335. [CrossRef]
26. Di Prisco, M.; Ferrara, L.; Lamperti, M. Double edge wedge splitting (DEWS): An indirect tension test to identify post-cracking behaviour of fibre reinforced cementitious composites. *Mater. Struct.* **2013**, *46*, 1893–1918. [CrossRef]
27. Baby, F.; Graybeal, B.; Marchand, P.; Toutlemonde, F. UHPFRC tensile behaviour characterization: Inverse analysis of four-point bending test results. *Mater. Struct.* **2013**, *46*, 1337–1354. [CrossRef]
28. Park, S.H.; Kim, D.J.; Ryu, G.S.; Koh, K.T. Tensile behavior of ultra high performance hybrid fiber reinforced concrete. *Cem. Concr. Compos.* **2012**, *34*, 172–184. [CrossRef]
29. Wille, K.; El-Tawil, S.; Naaman, A.E. Properties of strain hardening ultra high performance fiber reinforced concrete (UHP-FRC) under direct tensile loading. *Cem. Concr. Compos.* **2014**, *48*, 53–66. [CrossRef]
30. Baby, F.; Graybeal, B.; Marchand, P.; Toutlemonde, F. Proposed flexural test method and associated inverse analysis for ultra high performance fiber reinforced concrete. *ACI Mater. J.* **2012**, *109*, 545–556.
31. Hillerborg, A.; Modéer, M.; Petersson, P.E. Analysis of crack formation and crack growth in concrete by means of fracture mechanics and finite elements. *Cem. Concr. Res.* **1976**, *6*, 773–782. [CrossRef]
32. Conforti, A.; Zerbino, R.; Plizzari, G.A. Influence of steel, glass and polymer fibers on the cracking behavior of reinforced concrete beams under flexure. *Struct. Concr.* **2019**, *20*, 133–143. [CrossRef]
33. Conforti, A.; Zerbino, R.; Plizzari, G.A. Assessing the influence of fibers on the flexural behavior of reinforced concrete beams with different longitudinal reinforcement ratios. *Struct. Concr.* **2020**. [CrossRef]